PERGAMON

International Journal of Solids and Structures 39 (2002) 5495–5513

INTERNATIONAL JOURNAL OF SOLIDS and STRUCTURES

www.elsevier.com/locate/ijsolstr

Scattering coefficient reconstruction in plates using focused acoustic beams

D.E. Chimenti *, D. Fei

Department of Aerospace Engineering and Engineering Mechanics, Center for Nondestructive Evaluation, Iowa State University, 1200 Howe Hall, Ames, IA 50011-3042, USA

Received 1 October 2001; received in revised form 18 February 2002

Abstract

A method has been developed and proven using highly focused acoustic beams that allows for the rapid reconstruction of scattering coefficients of a thin anisotropic plate immersed in liquid. In a single bistatic coordinate scan, nearly the entire range of wave number within the spatial and temporal frequency bandwidth of the transducer can be reconstructed. This paper also reports the development of a multiple-source complex transducer point model that includes all extrinsic factors and permits prediction of the wave number-frequency (k–f) domain result obtained from a scan of focused transducers in a pitch-catch reflection or transmission arrangement. Extensive experiments have been performed to test the method and the model and to demonstrate transducer beam effects on the k–f domain results, leading to a very efficient method for mapping major portions of the guided wave dispersion spectrum in thin-plate media. As a demonstration of the technique, an estimate of material elastic properties in an isotropic and a transversely-isotropic plate is reported, making only minimal use of the highly redundant dispersion data. Acoustic velocities inferred from these experiments show a disparity of less than 3% from contact acoustic estimates of the same parameters in either plate.

Keywords: Lamb waves; Focused beams; Dispersion relation; Elastic properties

1. Introduction

The subject of materials characterization is a rich one, even when considered from the standpoint of ultrasonic methods only. It is a theme that encompasses not only the inference of elastic properties, mainly considered in this article, but also the study of defects, whether occurring discretely or in clusters, and their influence on elastic wave scattering measurements. In this latter area especially, Achenbach and his collaborators have contributed substantially over a period of decades. Their bibliography would easily outnumber all the other citations in this current article. From effective medium theories for composite laminates to property changes owing to cracks on surfaces and the scattering of Rayleigh waves, these are

* Corresponding author. Tel.: +1-515-294-5853; fax: +1-515-294-3262.
E-mail address: chimenti@iastate.edu (D.E. Chimenti).

0020-7683/02/$ - see front matter
PII: S0020-7683(02)00361-X

only a few of the many problems to which they have turned their productive attention. In addition, arrays of cracks and the integrated apparent changes such defect clusters bring to the elastic properties also have occupied Achenbach and his associates. Nonlinear phenomena, the materials characterization of micron-scale thin films, and how these questions might be brought to bear on the problem of adhesive bond assessment are yet further areas of their endeavor. In fact, the sheer breadth and depth of their work renders the prospect of a complete treatment of their contributions in this short introduction all but impossible. It is sufficient to say that those of us who study and explore material properties of solids with stress waves work very much in the long shadow cast by Professor Achenbach's achievements.

Many papers have appeared within the past ten years or so in which elastic properties of complex composite media have been the focus of the investigation. Rohklin and Chimneti (1990) conducted a detailed sensitivity analysis and demonstrated the advantages of isolating elastic property searches to areas of the plate wave dispersion where various elastic constants dominate the behavior. Hosten et al. (1987) studied lossy media using inhomogeneous waves, whereas Weaver et al. (1989) used transient waves generated by a point source to characterize composite laminates. Karim et al. (1990) attempted to fit all elastic stiffnesses at once to the result of selected Lamb wave measurements. An energy approach was taken by Karunasena et al. (1991) to calculate plate wave dispersion, and Deschamps and Hosten (1992) evaluated the effect of viscous damping on plate waves. Properties of thick composites were studied by Hsu and Margetan (1992) using acousto-ultrasonics, and through-transmission pulse propagation methods were applied by Rokhlin and Wang (1992) to deduce the elastic stiffnesses of plates, without appealing to complicated group-velocity methods. Point-source and point-receiver techniques, reminiscent of acoustic emission, were used by Veidt and Sachse (1994) to demonstrate plate wave propagation in composites. A method related to the one reported here was proposed by Rogers (1995), in which a two-point phase-sensitive measurement along the lines of Sachse and Pao (1978) was used to infer Lamb wave phase velocities in isotropic plates more accurately than could be done by observing incident angles. Rogers also pointed out the advantage of property searches limited to specified regions of the dispersion relations. A synthetic-aperture method to capitalize on information contained in the spatial-frequency spectrum was introduced by Safaeinili et al. (1996) to characterize viscoelastic properties of plastics and composites in air-coupled measurements. Further such experiments in air were carried out by Hosten et al. (1996). Minachi et al. (1994) used acousto-ultrasonics to characterize a thick composite plate. An extension of the synthetic-aperture scanning in fluid-coupled experiments by Lobkis et al. (2000) demonstrated a robust technique to estimate the large in-plane composite stiffness. Although a number of works are cited here, space limitations preclude the mention of many other contributions. A recent review article by Chimenti (1997) includes further discussion of much of this additional work.

In a conventional leaky wave measurement, two identical planar transducers at the same orientation angle are used, in a pitch-catch reflection or transmission arrangement. The output voltage of the receiver transducer in such measurements inevitably contains contributions from both intrinsic material properties and extrinsic experimental parameters. The intrinsic contribution can be isolated to the plane-wave reflection coefficient (RC) or transmission coefficient (TC), or more generally the scattering coefficient (SC), which depends only on the measurement frequency and the material properties of the plate and the coupling fluid. The extrinsic parameters include all the experimental settings, such as the aperture size, beam shape, orientation angle, and position of the transmitting and receiving transducers. Because the extrinsic contributions can be substantial, modeling of the receiver output voltage and a careful study of the extrinsic effects on the measurement results have become important issues in accurate elastic property determination. In a two-transducer geometry Lobkis et al. (1996) and Lobkis and Chimenti (1999) have used the plane-wave decomposition of an incident planar beam and the reciprocity theorems of Kino (1978) and Auld (1979) to derive a theoretical expression for the receiver output voltage as a function of frequency, SC, transducer position, and phase-match angle. These researchers (Lobkis et al., 1996) have demonstrated that although the acoustic field of a piston transducer is very different from a Gaussian beam, the combined

directivity functions of an identical planar transmitter and receiver can be replaced accurately by those of two Gaussian acoustic beams. The geometrical dependence of the receiver voltage also was studied (Lobkis et al., 1996), as well as the influence of the 3-D beam effects (Lobkis and Chimenti, 1999).

Complex source points (CSP), introduced first by Deschamps (1971), provide a simple mathematical approach for constructing Gaussian beams. The simplest acoustic generator is the point source. Beams, by contrast, can be considered either collections of Huygen's wavelets or spectra of plane waves, but in any case much more complicated than a point source. Deschamps found, however, that by displacing a real point source into the complex plane, the resulting wave field is almost identical to a Gaussian beam. Because this field source is reciprocal, it may be viewed as a receiver as well. A combination of complex source and receiver points has, therefore, been termed "complex transducer points" (CTP) (Zeroug et al., 1996). Chimenti et al. (1994), and Zeroug and Felsen (1994, 1995) have used the Gaussian beams to study the interaction of acoustic beams with both planar and cylindrical structures. Recently, Zhang et al. (1998) and Zhang and Chimenti (2000) have applied the CTP approach to analyze geometric effects on the receiver voltage (Zhang et al., 1998) and to investigate the differences between the 2-D and 3-D voltage calculation for fluid-coupled reflection experiments (Zhang and Chimenti, 2000). All the above studies, however, are limited to the configuration in which an identical planar transmitter and receiver are used. The extrinsic effects on the measurement results owing to source curvature have not been investigated, although Zeroug et al. (1996) have pointed out that the CTP approach also is applicable to the modeling of focused transducers.

In our own recent work (Fei and Chimenti, 2001) we have employed highly focused transducers to obtain a rapid estimation of the RC efficiently and to use its associated plate wave dispersion spectrum to deduce the elastic property of the plate material. We exploit the wide angular beam spread of highly focused transducers to generate a broad spatial frequency spectrum, permitting us to map in a single coordinate scan the zeroes of the plate RC using a synthetic aperture scan technique developed in earlier work (Safaeinili et al., 1996). In this technique the receiver transducer is scanned parallel to the plate and the output voltage signal is sampled in time at every scan position. The x–t (space-time) domain data collected in a scan are then transformed into the k–f (wave number-frequency) or θ–f (phase-match angle-frequency) domain using combined temporal and spatial Fourier transforms. Similar methods have been used previously by Sachse and Pao (1978) for measuring group and phase velocities of dispersive Lamb waves and by Alleyne and Cawley (1991) for analyzing the scattered signals from defects in plates.

In this paper we report an experimental procedure using focused transducer beams to measure scattering (reflection or transmission) coefficients. We provide a sophisticated theoretical model to explain in detail the transducer beam effects on the measurements based on a weighted sum of Gaussian beams, simulated by CSPs and complex receiver points, or more generally, CTPs. This additional effort is necessary because the effect of the focussing is to suppress the phase averaging experienced when the field of a piston radiator is measured by a second identical piston. In fact, for two identical focused probes in a confocal geometry, the measured voltage at any frequency or position is essentially identical to that produced by the field of either device and sampled by a point receiver (Kolosov et al., 1993; Levin et al., 1990). We first discuss the model calculation, followed by the experimental procedure, and finally the results.

2. Model calculation

To study the transducer beam effects completely, we allow either transducer (the transmitter or the receiver) to be either planar or focused, to have variable aperture size, to be oriented at unequal incident angles, and to have variable vertical distance from the plate. The geometric configuration used in the experiment and model calculation is shown in Fig. 1. Both transducers are focused: the transmitter has a radius of a' and a focal length of F_0', and the receiver has a radius of a and a focal length of F_0. Other cases,

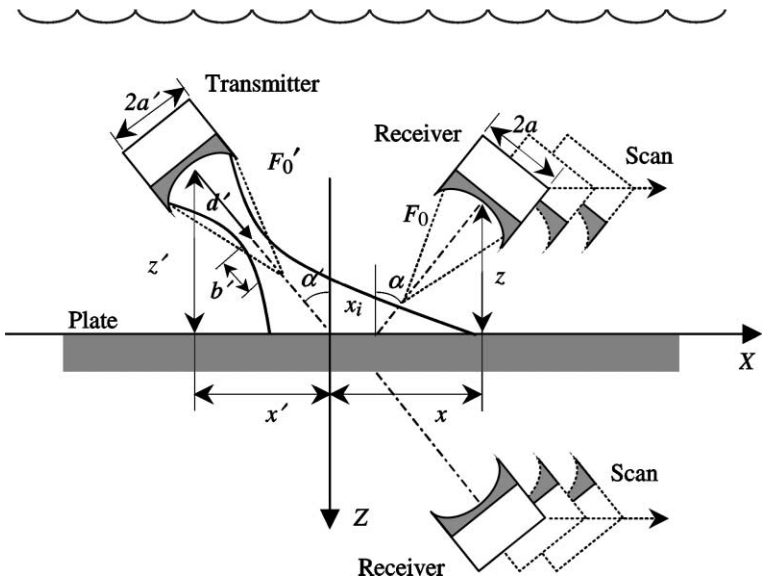

Fig. 1. Geometric configuration used in the experiment and model calculation showing transducer focusing parameters.

in which both transducers or one of the two transducers are planar, also will be investigated. In fact, because a planar transducer can be regarded as a curved aperture with an infinite focal length, the planar and focused transducers can both be treated as focused transducers in the model. The transmitter and receiver are respectively oriented at α' and α with respect to the positive Z-axis. The distances from the transducer aperture centers to the plate are z' and z, respectively, for the transmitter and receiver. In our calculations, we make no assumptions concerning the equality of a' and a, α' and α, or z' and z. Each of these pairs of experimental parameters can be equal or unequal.

In the following, we first apply the CTP approach to model the transmitter and receiver and derive a theoretical expression of the receiver output voltage for a single frequency and receiver position. We then analyze the synthetic-aperture scan method and reach the theoretical prediction for the output voltage in the k–f domain, where the comparison between model and experiment is to be made. In the last section we extend the model by employing multiple CTPs to calculate accurately the sidelobe behavior of the focused probes.

2.1. Complex transducer point

A linear, electro-acoustically reciprocal Gaussian beam transducer, either planar or focused, serving as either a transmitter or a receiver, can be replaced with a CTP by displacing the transducer from its position at a real spatial coordinate to a complex spatial coordinate, according to the following operation (Zeroug et al., 1996),

$$\boldsymbol{r} \to \tilde{\boldsymbol{r}} = \boldsymbol{r} + \boldsymbol{d} + i\boldsymbol{b}, \tag{1}$$

where vector $\boldsymbol{r} = (x, y, z)$ is the location of the transducer aperture center, vector $\tilde{\boldsymbol{r}} = (\tilde{x}, \tilde{y}, \tilde{z})$ is a complex vector that specifies the location of the CTP in the complex plane, vector $\boldsymbol{d}$ is the location of the Gaussian beam waist of the transducer relative to the transducer aperture center, and vector $\boldsymbol{b}$ specifies the transducer beam direction and its Fresnel length, as shown in Fig. 1. The directions of vectors $\boldsymbol{d}$ and $\boldsymbol{b}$ are the same: both are in the beam direction. The magnitude of vector $\boldsymbol{b}$, or the Fresnel length b, is related to the $1/e$

beamwidth at the waist location W through $b = (1/2)k_f W^2$, where $k_f (= \omega/c_f)$ is the fluid wave number, ω is the circular frequency, and c_f is the sound speed in the coupling fluid. The beam width at the waist location W and the distance between the waist location and the transducer aperture center d (which is also the magnitude of vector $\boldsymbol{d}$) are given by (Thompson and Lopes, 1984),

$$W = W_0 \frac{\beta}{(1+\beta^2)^{1/2}}, \quad d = \frac{F_0}{1+\beta^2}, \tag{2}$$

where $\beta = 2F_0/(k_f W_0^2)$, F_0 is the transducer focal length, and W_0 is the beam width at the transducer aperture. A good estimation of W_0 has been given by $W_0 = 0.752a$ (Thompson and Lopes, 1984; Lobkis et al., 1996) for measurements near or larger than the Rayleigh distance a^2/λ, where a is the radius of the transducer aperture and $\lambda = c_f/f$ is the wavelength in the coupling fluid. For planar transducers we simply let F_0 be infinite, and we have $d = F_0/(1+\beta^2) = k_f^2 W_0^4 F_0/(k_f^2 W_0^4 + 4F_0^2) \to 0$, which means the beam waist is at the aperture center, and thus $W = W_0$.

2.2. Output voltage in the x–f domain

To model the output voltage of the receiver in the configuration shown in Fig. 1, we substitute both the transmitter and receiver beams by CTPs, and we have the following complex coordinates, respectively, for the transmitter (primed) and receiver (unprimed),

$$\tilde{x}' = x' + d'\sin\alpha' + \mathrm{i}b'\sin\alpha', \quad \tilde{y}' = y', \quad \tilde{z}' = z' + d'\cos\alpha' + \mathrm{i}b'\cos\alpha', \tag{3}$$

$$\tilde{x} = x - d\sin\alpha - \mathrm{i}b\sin\alpha, \quad \tilde{y} = y, \quad \tilde{z} = z \pm (d\cos\alpha + \mathrm{i}b\cos\alpha), \tag{4}$$

where the positive of the $\pm$ is taken for reflection and the negative for transmission. The above equations can be further simplified if the transducer is planar. We maintain them in a general form, however, so that the following discussion is applicable to both planar and focused transducers.

By applying the reciprocity theorem of Kino (1978) and Auld (1979) and using the angular spectrum decomposition of the complex transmitter and receiver points, we get the following output voltage $V(x,f)$ for a single receiver position x and measurement frequency f (Zeroug et al., 1996; Zhang and Chimenti, 2000),

$$V(x,f) = -\frac{1}{8\pi^2}\gamma(\omega)\omega\rho_f \int_{-\infty}^{\infty}\int_{-\infty}^{\infty} S(k_x,k_y,f)\frac{\exp[\mathrm{i}k_x(\tilde{x}-\tilde{x}') + \mathrm{i}k_y(\tilde{y}-\tilde{y}') - \mathrm{i}k_z(\tilde{z}\pm\tilde{z}')]}{k_z}\mathrm{d}k_x\mathrm{d}k_y, \tag{5}$$

where $\gamma(\omega)$ is the combined frequency response of both transducers and the associated electronics (or the system efficiency factor (Schmerr, 1998)), ρ_f is the mass density of the coupling fluid, S is the plane-wave SC of the fluid-loaded plate, and k_x, k_y and $k_z (= (k_f^2 - k_x^2 - k_y^2)^{1/2})$ are, respectively, the x, y and z components of the wave vector of an angular spectrum plane-wave component.

From this point on, we limit our model calculation to the 2-D case in which both the transmitter and receiver have a 2-D beam distribution in the x–z plane, i.e., a sheet beam. The output voltage therefore has no y dependence and becomes,

$$V(x,f) = -\frac{1}{4\pi}\gamma(\omega)\omega\rho_f \int_{-\infty}^{\infty} S(k_x,0,f)\frac{\exp[\mathrm{i}k_x(\tilde{x}-\tilde{x}') - \mathrm{i}k_z(\tilde{z}\pm\tilde{z}')]}{k_z}\mathrm{d}k_x, \tag{6}$$

where $k_z = \sqrt{k_f^2 - k_x^2}$.

2.3. Output voltage in the k–f domain

The expression for the k–f domain voltage $V(k,f)$ derived from coordinate scan data is obtained by performing a spatial Fourier transform on the x–f domain voltage given by Eq. (6),

$$V(k,f) = \int_{-\infty}^{\infty} V(x,f)\exp(-\mathrm{i}kx)\mathrm{d}x. \tag{7}$$

Because $V(x,f)$ above contains an integration over wave number, the expression in Eq. (7) requires evaluation of two integrals. Evaluating the integral over the x coordinate above yields $2\pi\delta(k_x - k)$, where δ is the Dirac delta function. After calculating the second integral over k_x, we have

$$V(k,f) = -\frac{1}{2}\gamma(\omega)\omega\rho_{\mathrm{f}}S(k,0,f)\frac{\exp\{\mathrm{i}k[-(d+\mathrm{i}b)\sin\alpha - \tilde{x}'] - \mathrm{i}k_z(\tilde{z}\pm\tilde{z}')\}}{k_z}, \tag{8}$$

where again, the positive sign of the $\pm$ is for reflection and the negative sign for transmission. We further substitute the complex coordinates given by Eqs. (3) and (4) into the exponential term in Eq. (8). With simplification, the exponential term in Eq. (8) can be cast in the form

$$\begin{aligned}\exp\{\mathrm{i}k[-(d+\mathrm{i}b)\sin\alpha - \tilde{x}'] - \mathrm{i}k_z(\tilde{z}\pm\tilde{z}')\} = \exp\{&k_{\mathrm{f}}[b\cos(\theta-\alpha) + b'\cos(\theta-\alpha')] \\ &- \mathrm{i}k_{\mathrm{f}}[x'\sin\theta + (z\pm z')\cos\theta + d\cos(\theta-\alpha) + d'\cos(\theta-\alpha')]\},\end{aligned} \tag{9}$$

where $\theta(=\sin^{-1}[k/k_{\mathrm{f}}])$ is the phase-match angle, or the incident angle of a plane-wave component in the beam of the transmitting transducer. If we consider only the magnitude of $V(k,f)$, we have for Eq. (8)

$$\begin{aligned}|V(k,f)| &= \frac{1}{2}\gamma(\omega)\omega\rho_{\mathrm{f}}|S(k,0,f)|\frac{\exp\{k_{\mathrm{f}}[b\cos(\theta-\alpha) + b'\cos(\theta-\alpha')]\}}{k_{\mathrm{f}}\cos\theta} \\ &\cong \frac{1}{2}\gamma(\omega)\omega\rho_{\mathrm{f}}|S(k,0,f)|\frac{\exp[k_{\mathrm{f}}(b+b')]\exp[-k_{\mathrm{f}}b(\theta-\alpha)^2]\exp[-k_{\mathrm{f}}b'(\theta-\alpha')^2]}{k_{\mathrm{f}}\cos\theta}.\end{aligned} \tag{10}$$

Eqs. (8)–(10) show the effects of the extrinsic experimental parameters on the k–f domain output voltage. First, we can see that the vertical positions of the transmitter and receiver, respectively z' and z, influence only the phase, not the magnitude of the k–f domain output voltage. Second, we can see how the properties of the acoustic beams from the transmitter and receiver affect the angular range of the k–f domain result. Both the transmitter and receiver beams have a Gaussian distribution profile centered on a beam axis whose orientation is determined by the transducer orientation angle. The beam width $\Delta\theta$, which is given by $\Delta\theta = (2k_{\mathrm{f}}b)^{-1/2} = (k_{\mathrm{f}}W)^{-1}$, is determined by the transducer Fresnel length b (or the beam waist width W) for a given frequency and coupling fluid. The smaller the Fresnel length, the larger the angular spread of the transducer beam. In the output voltage, the combined contribution from the transmitter and receiver beams is a product of the individual contributions. In the case of an identical transmitter and receiver at the same orientation angle, we will have $b' = b$ and $\alpha' = \alpha$, and consequently,

$$|V(k,f)| = \frac{1}{2}\gamma(\omega)\omega\rho_{\mathrm{f}}|S(k,0,f)|\frac{\exp(2k_{\mathrm{f}}b)\exp[-2k_{\mathrm{f}}b(\theta-\alpha)^2]}{k_{\mathrm{f}}\cos\theta}. \tag{11}$$

If the two Fresnel lengths are both zero, the output voltage in the k–f domain contains no beam effects, because energy in the two transducer beams is uniformly distributed over the entire angular range. This implies an ideal measurement where the SC over the entire angular range can be reconstructed from a single transducer scan. The only limitation is the frequency range, which is determined by the electronic response $\gamma(\omega)$.

Practically speaking, it is not possible for the Fresnel length of a transducer to be zero, but it is possible for the Fresnel length to be very small. According to Eq. (2) and the estimate for $W_0(\cong 0.752a)$, a small

Fresnel length can be achieved at constant frequency either by decreasing the transducer aperture size a while maintaining the ratio of a/F_0 constant, or by decreasing the focal length F_0 while maintaining the aperture size a constant. The former relies on the transducer diffraction effect, and the latter relies on the beam focusing effect, whereas both increase the angular beam spread of the transducer. The angular beam spread of a finite aperture of radius a owing to the diffraction effect is the order of λ_f/a (Schmerr, 1998), where $\lambda_f(= c_f/f)$ is the wavelength in the coupling fluid. In a typical leaky wave measurement, λ_f is about 0.3 mm. To achieve an angular beam spread of tens of degrees, the transducer aperture size a needs to be 1 mm or smaller. Such small transducers generate beams of low power and lead to low detection sensitivity, besides being difficult to make. On the other hand, using beam focusing is a much more effective way to achieve a small Fresnel length and a large angular beam spread. By using focused transducers with a high ratio of a/F_0, an angular beam of tens of degrees can be obtained easily. These highly focused transducers can be used to make rapid measurements of the SC over a large angular range.

2.4. Multiple-CTP model

In the single-CTP model described above, each transducer is substituted with a single CTP that has a Gaussian beam profile with no sidelobes. To include the influence of sidelobes in the model, we use multiple CTPs to substitute for both transducers. The k–f domain output voltage is the summation of all the possible interactions between the individual CTPs of the transmitter and receiver. It can be shown that the magnitude of the k–f domain receiver voltage becomes

$$|V(k,f)| = \frac{1}{2}\gamma(\omega)\omega\rho_f|S(k,0,f)|\frac{1}{k_f\cos\theta} \times \left|\sum_{m=1}^{N}\sum_{n=1}^{N} A_m A_n \tilde{\mathbf{x}}'_m \tilde{\mathbf{x}}_n \exp[-ik_f\{\tilde{\mathbf{x}}'_m[\cos(\theta-\alpha')-1]+\tilde{\mathbf{x}}_n[\cos(\theta-\alpha)-1]\}]\right|, \tag{12}$$

where N is the total number of CTPs for either the transmitter or receiver, $\tilde{\mathbf{x}}'_m$ and $\tilde{\mathbf{x}}_n$ ($m, n = 1, 2, \ldots, N$) are the complex coordinates of the individual CTPs of the transmitter and receiver, respectively, and A_m ($m = 1, 2, \ldots, N$) are the coefficients of the mth CTP. A convenient way to determine the coefficients A_m and the beam waist W_{0m} of the mth CTP for either transducer is to use the parameters of the individual Gaussian beam in a multiple-Gaussian beam model, because of the close relationship between a CTP and a Gaussian beam. In this work we assume that $N = 10$ and use Wen and Breazeale (1988) constants A_m and B_m ($m = 1, 2, \ldots, 10$). We have found that their coefficients A_m can be used directly. The beam waist parameters B_m need to be converted, however, into W_{0m}, according to $W_{0m}^2 = a^2/B_m$, where a is the transducer radius. The parameters W_{0m} ($m = 1, 2, \ldots, 10$) are further used in Eqs. (2)–(4) to calculate the complex coordinates of the transmitter and receiver that are required in Eq. (12).

3. Experimental procedure

Experiments have been performed in a Parker–Daedel scanning system with precision linear control. The system has a spatial resolution of 0.01 mm. Both the transmitter and receiver transducers are mounted on precision rotary stages with a usable angular resolution of 0.01°. A pulse/receiver (Panametrics 5052PR) is used to provide a wide-band (about 28 MHz) electronic impulse to the transmitter. The output voltage of the receiver transducer, after being amplified from 10 to 20 dB, is acquired by a Lecroy 9304 digitizing oscilloscope. A digital delay/pulse generator (Stanford Research Systems, DG 535) is used to produce a delayed trigger signal to the oscilloscope so that the output signal appears within the oscilloscope screen

window after its propagation in water path. Two plate specimens have been used: one is a 1.60-mm-thick isotropic aluminum plate with a measured longitudinal wave velocity of 6.38×10^3 m/s, a shear wave velocity of 3.10×10^3 m/s, and a density of 2.78×10^3 kg/m^3; the other is a 0.92-mm-thick 8-ply uni-axial T300/CG-914 graphite–epoxy laminate with a density of 1.60×10^3 kg/m^3.

To perform a coordinate scan, the receiver transducer is scanned along the plate while the other geometric parameters are held constant, as shown in Fig. 1. The output voltage is sampled as a time signal at each coordinate position. The scan step and the sampling time interval are respectively much less than the smallest wavelength and the time period of the guided wave modes of interest. The scan step varies from 0.1 mm to 1.0 mm, depending on the transducer type, orientation, and position. The total number of scan steps is about 200. The received *RF* signal is digitized into 500 points of data at a typical sampling frequency of 25 MHz (for 2 μs/div) or 50 MHz (for 1 μs/div) and is averaged 64 times. The time window and the scan range are set to be large enough to collect all the receiver output signals of signal-to-noise ratio greater than about unity. The output signals lying outside of the time and spatial ranges are very small (typically smaller than 2–3% of the largest signal amplitude in a scan) and can be ignored. Therefore, the scan ranges are effectively infinite in both time and space ranges. A PC with a user interface developed using LabVIEW (National Instruments, TX) has been used to control the measurement process. The acquired receiver output voltage data are further processed using Fortran and MATLAB (Math Works, MA) programs. A more detailed description of the experimental system and the measurement procedure can be found in the thesis by Fei (2001).

4. Results and discussion

4.1. Effects of transducer beam focusing

The effects of transducer beam focusing on the k–f domain result obtained from a synthetic-aperture transducer scan are demonstrated on the 1.60-mm-thick isotropic aluminum plate in the reflection arrangement. We start our discussion with the case in which both the transmitter and receiver transducers are planar, then study the case of a planar and focused transducer, and finally discuss the focused transmitter and focused receiver case.

4.1.1. Planar–planar case

In this case both the transmitter and receiver transducers are planar; a typical example is the conventional leaky wave measurement. Fig. 2 shows a set of synthetic-aperture scan results in a measurement, where the two planar transducers are identical, oriented at identical angles, and positioned at the same distance from the plate. The transducers are a pair of 5 MHz planar probes with a diameter of 9.53 mm. The orientation angles of the two transducers are both 10°, and the vertical distances of the two transducers from the plate are both 100 mm. The coordinate scan is performed for x_i from −20.0 to 20.0 mm at a step of 0.2 mm. The sampling frequency is 25 MHz and the time window is 20 μs wide. Fig. 2(a) shows the raw scan data in the x–t domain plotted as a grayscale image, where the brightness is proportional to the magnitude of the acquired output voltage. The curved trace indicated by the high amplitude is the front-surface echo from the plate. The trailing leaky signals are also observable, but of much smaller magnitude. The entire reflected field from the plate has been collected in both the time and spatial windows of the scan.

After two consecutive Fourier transforms are performed, first in the t coordinate and then in the x coordinate, the x–t domain data shown in Fig. 2(a) are transformed in the k–f domain. The result is shown in Fig. 2(b) as an image with the brightness proportional to the absolute value of the data in dB (Yang and Chimenti, 1995). In the k–f domain, a line through the origin has a constant slope of k/f, which corresponds uniquely to a phase-match angle θ in the coupling fluid according to $\theta = \sin^{-1}(c_f k/2\pi f)$. We label

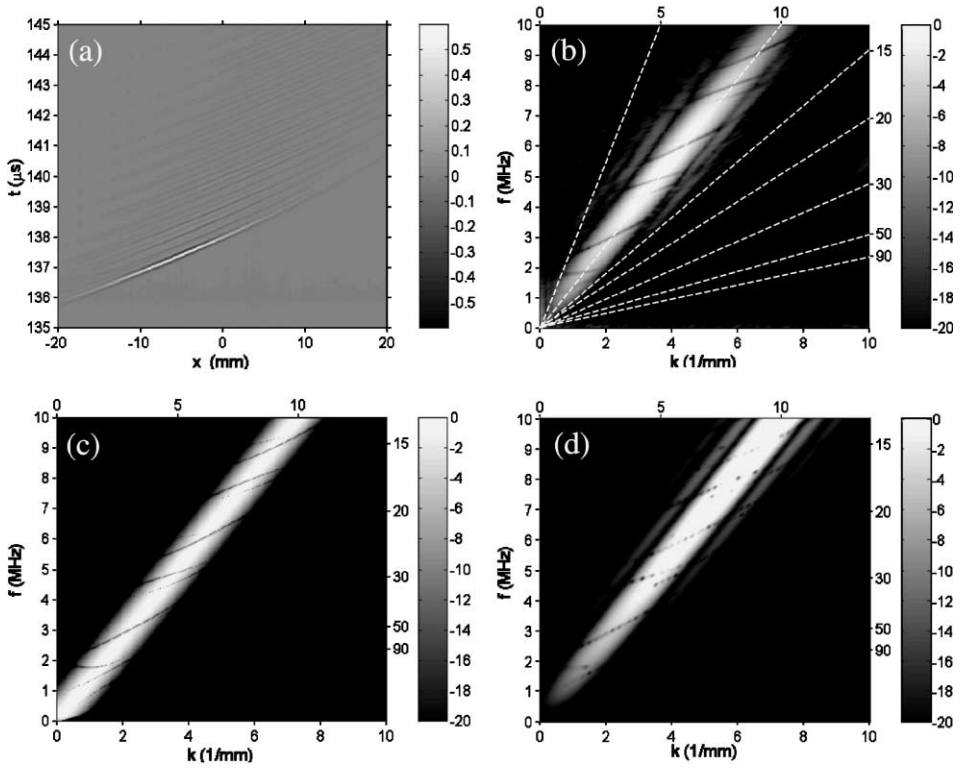

Fig. 2. Comparison between experimental and model results for a pair of planar transducers at 10°: (a) raw scan data in the x–t domain, (b) experimental k–f domain result, (c) single-CTP model prediction, and (d) multiple-CTP model prediction.

the phase-match angles at the upper and right edges of the image to indicate clearly the angular range of the k–f domain result. In Fig. 2(b) the region of high amplitude is concentrated along 10°, which is the orientation angle of the transmitter and receiver. Tracing the data at minimum amplitude we can see the dispersion curves of several guided wave modes. Because the beams of the planar transmitter and receiver are both highly collimated, however, only a very narrow portion of the dispersion spectrum has been mapped out.

The k–f domain prediction by the single-CTP model is shown in Fig. 2(c). By comparison with (b), we see that the model calculation agrees well with the experimental result. In both figures the high-amplitude region has a nearly constant cross-sectional width, which can be explained using the model we have developed. Based on Eq. (11), we can determine the following $1/e$ angular beam width $\Delta\theta$,

$$\Delta\theta = \frac{1}{\sqrt{2k_f b}} = \frac{1}{k_f W} \cong \frac{c_f}{1.504\pi a f}. \tag{13}$$

The cross-sectional width of the high-amplitude region is proportional to $f\Delta\theta$ and is therefore constant. Note that the approximation in the above equation comes from the beam waist assumption for planar transducers, i.e., $W \cong 0.752a$. The fact that the high-amplitude region in Fig. 2(c) has a nearly constant width from below 1–10 MHz shows in turn that this assumption is valid across a wide frequency range.

The model prediction by the multiple-CTP model is shown in Fig. 2(d), from which we see the sidelobe effects in the vicinity of the main high-amplitude region. This structure agrees with the experimental observation shown in Fig. 2(b), but does not appear in the prediction of the single-CTP model (Fig. 2(c)) for

the obvious reason: Gaussian beams of the CTP model have no sidelobes. Even for identical planar piston transducers, the sidelobe effects in the voltage are very small, owing to the averaging of the signal phase over the receiver surface in the reception process (Lobkis et al., 1996).

The sidelobe effects become more prominent when the orientation angles of the transmitter and receiver do not match each other. Fig. 3(a) and (b) show the experimental k–f domain results for the receiver at 12° and 15°, respectively. The transmitter is at 10° in both measurements. By comparison it can be seen that the k–f domain result is very sensitive to the transducer orientation. As the receiver orientation angle differs from the transmitter orientation angle, we start to see significant sidelobe effects from both transducers. This is especially evident in Fig. 3(b), where the sidelobe nulls from the transmitter appear at a receiver

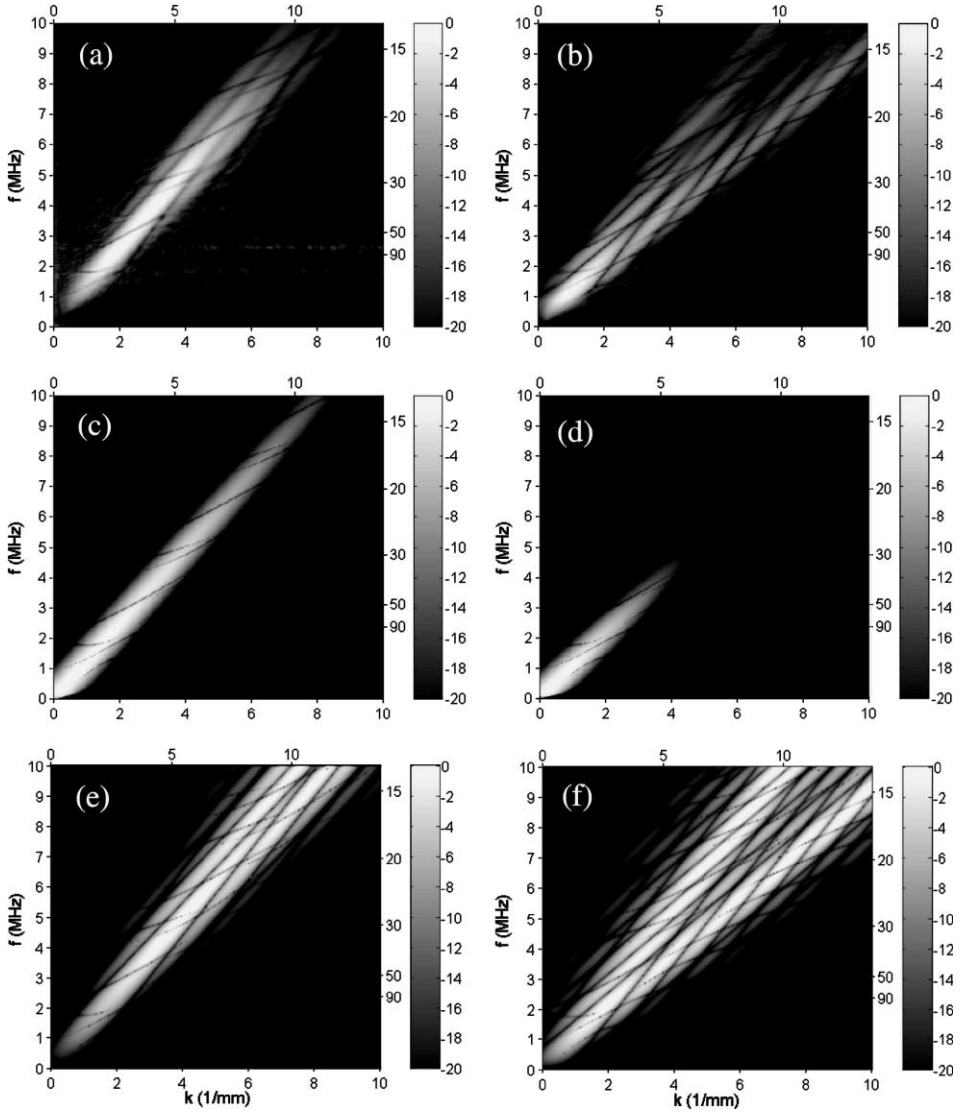

Fig. 3. Comparison between experimental and model results for a pair of planar transducers at different angles. The transmitter is at 10°. The receiver is at 12° in (a), (c), and (e) and at 15° in (b), (d), and (f). (a) and (b) are experimental k–f domain results; (c) and (d) are single-CTP model predictions; (e) and (f) are multiple-CTP model predictions.

orientation angle of 15°, and the sidelobe effects of the receiver appear at a transmitter orientation angle of 10°. The two transducers have slightly different generation/detection efficiencies and other minor differences that arise in fabrication. Individual tests on each transducer show that the transmitter is slightly more efficient than the receiver and has stronger sidelobe behavior. The measurement combines these two efficiencies inextricably, so the relative contributions to the sidelobe effects cannot be separated, even though the influence of the transmitter is evidently stronger than that of the receiver. Fig. 3(c) and (d) show the predictions by the single-CTP models for the above two measurements, respectively. Fig. 3(e) and (f) are the multiple-CTP model predictions for the above two measurements. The single-CTP model has predicted many features of the experimental results. In the lower frequency range, the transmitter and the receiver have relatively large angular beam spreads. The output voltage is therefore relatively insensitive to the mismatch between the transducer orientations. As the frequency increases and the transmitter and receiver beams become more and more collimated, the output voltage decreases. The single-CTP model, however, does not predict any sidelobe-related behavior observed experimentally, again because each transducer has been modeled as a single CTP or Gaussian beam having no sidelobes. The multiple-CTP model, on the other hand, predicts well the sidelobe effects for both measurements.

4.1.2. Planar–focused case

In the planar–focused case one of the two transducers, either the transmitter or the receiver, is planar, and the other is focused. In the example shown in Fig. 4, both the planar and focused transducers have a center frequency of 5 MHz and are oriented at 10°. The planar transducer has a diameter of 9.53 mm. The

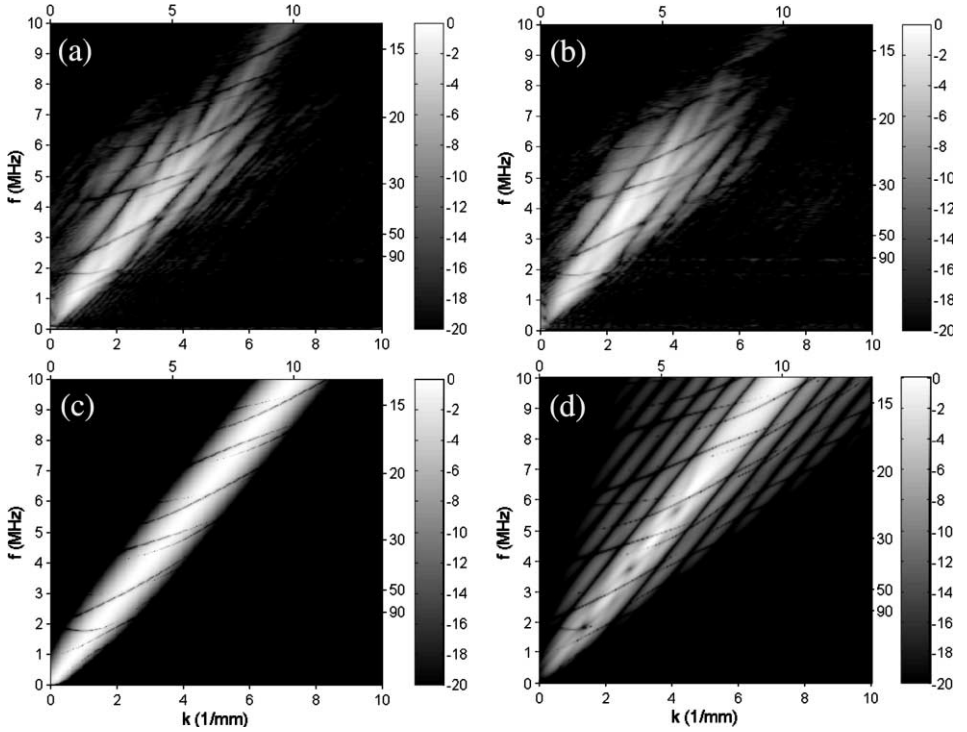

Fig. 4. Comparison between experimental and model results for a planar and focused transducer at 10°: (a) experimental, transmitter is planar and receiver is focused, (b) experimental, transmitter is focused and receiver is planar, (c) single-CTP model prediction, and (d) multiple-CTP model prediction.

focused transducer has a diameter of 25.4 mm and a focal length of 102 mm. Fig. 4(a) and (b) show the measured k–f domain results for the planar transmitter and focused transmitter, respectively. The fact that the two results are nearly identical gives a dramatic experimental confirmation of the reciprocity principle. In both results the strong central-lobe data appear at the transducer orientation angle 10°, which is the same as in the planar–planar case. Unlike the previous case, however, we see strong sidelobe effects, mainly from the planar transducer. When the receiver is focused, it detects the structure of the reflected acoustic field of the planar transducer (Gavrilov et al., 1988; Levin et al., 1990), including both the mainlobe and sidelobes. When the transmitter is focused, it emits a large angular range of incident wave components. The planar receiver detects reflected plane-wave components in both its mainlobe and sidelobes.

The prediction by the single-CTP model is shown in Fig. 4(c). The high-amplitude region has a nearly constant cross-sectional width, which is mainly determined by the planar transducer because the focused transducer has a much wider angular beam spread than the planar transducer. The cross-sectional width in this case is larger than that in Fig. 2(c) where both the transmitter and receiver are planar for the same reason. The prediction by the multiple-CTP model is shown in Fig. 4(d), from which we can see that the experimentally observed sidelobe behavior has been well predicted.

4.1.3. Focused–focused case

In this case both the transmitter and receiver probes are focused. The procedure for data collection and analysis, however, is essentially identical to that used for the results presented above. Fig. 5 shows two sets of experiment and model results: (a), (c) and (e) are for a pair of 5 MHz transducers (25.4 mm in diameter and 102 mm in focal length) at the same orientation angle of 12°; (b), (d) and (f) are for a pair of 2.25 MHz transducers (19.1 mm in diameter and 25.4 mm in focal length) at 24°. The synthetic aperture scans have been performed in a near confocal geometry. The receiver transducer is positioned with its focal point at the upper surface of the plate sample. The transmitter is positioned to allow for some overlap between the two transducers. The exact vertical positions of the transmitter and receiver are found not to be critical, as long as the two transducers are not too far from the sample. The experimental k–f domain results for the 5- and 2.25-MHz transducer pairs are shown in Fig. 5(a) and (b), respectively. We can see that both results are significantly different from our previous observations in the planar–planar or planar–focused cases. In this case the angular beam width $\Delta\theta$ of both transducers is given by

$$\Delta\theta = \frac{1}{k_f W} = \frac{1}{k_f W_0 \frac{\beta}{\sqrt{1+\beta^2}}} \cong \frac{1}{k_f W_0 \beta} = \frac{W_0}{2F_0} \cong 0.376\frac{a}{F_0}. \tag{14}$$

Hence, $\Delta\theta$ is independent of frequency, which explains why we see a constant angular span in the k–f domain results shown in Fig. 5(a) and (b). Note that the first approximation in the above equation is valid under the assumption that β, which is equal to $2F_0/k_f W_0^2$, is far smaller than the unity. This assumption is valid when the measurement frequency is high; it allows us to ignore the diffraction effect of a finite aperture so that the angular beam spread of the transducer depends only on the ratio of the aperture size a to the focal length F_0. For typical immersion experiments at several MHz, this is a good assumption (Thompson and Lopes, 1984; Levin et al., 1990).

Because the focused transmitter and receiver both have a wide angular beam spread, we get a much wider view of the RC and its associated dispersion spectrum than in the planar–planar or planar–focused cases. For the result shown in Fig. 5(a), the angular range is roughly from 6° to 18°. The angular range can be larger if the two focused transducers had a higher ratio of a to F_0. Common commercially available focused transducers can have an a/F_0 ratio of about 0.375, which gives a usable angular beam spread of about 45°. With such highly focused transducers, almost the entire angular range accessible by phase-matched fluid coupling can be measured in a single synthetic aperture scan with the transmitter and receiver at one orientation angle. Fig. 5(b) gives one example. Because this pair of transducers has a high a/F_0 ratio,

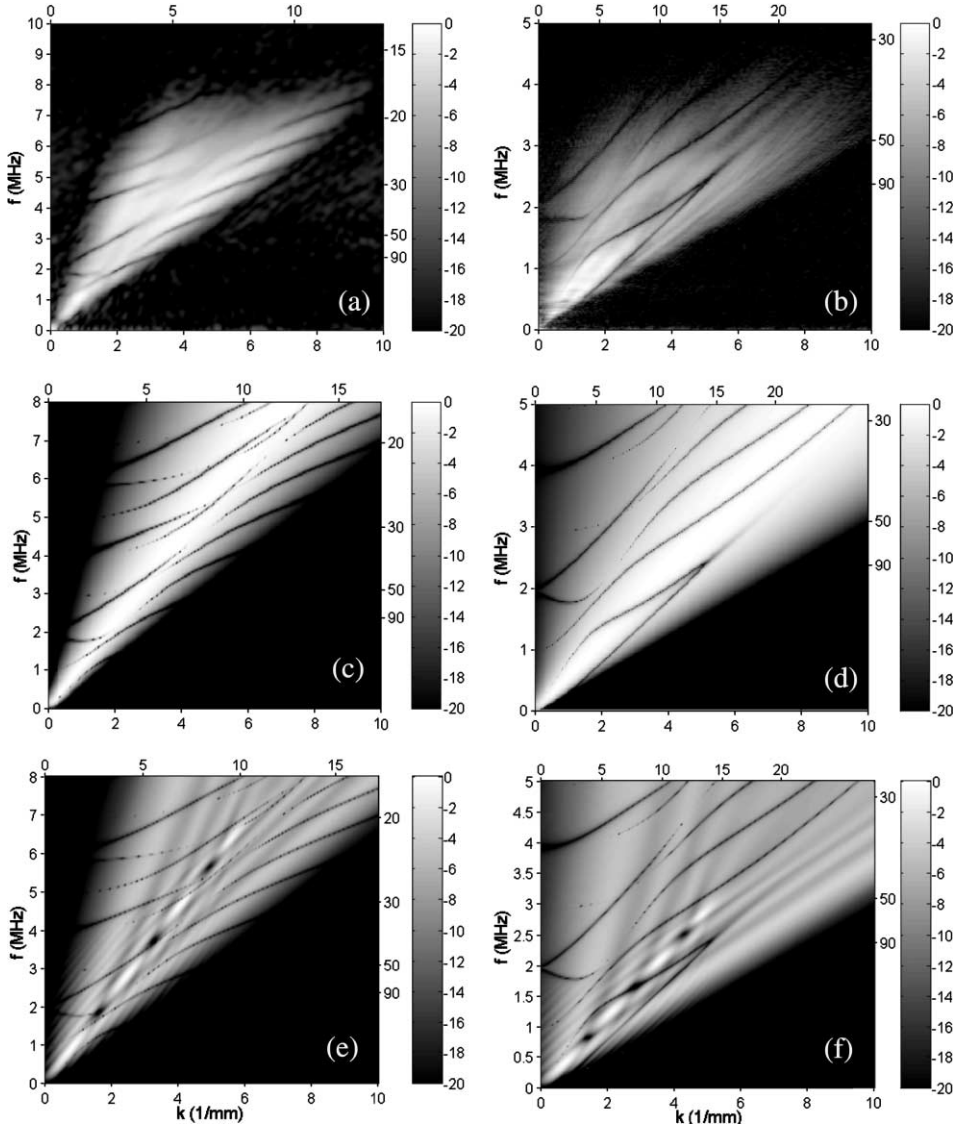

Fig. 5. Comparison between model and experimental results for two pairs of focused transducers. The transducers are a pair of 5 MHz, 25.4 mm diameter, and 102-mm focal length transducers at 12° in (a), (c), and (e), and a pair of 2.25 MHz, 19.1 mm diameter, and 25.4 focal length transducers at 24° in (b), (d) and (f). (a) and (b) are experimental k–f domain results; (c) and (d) are single-CTP model predictions; (e) and (f) are multiple-CTP model predictions.

we are able to map out the dispersion spectrum for phase-match angles as small as 3°, quite near to the mode cut-offs, and as large as 45°, well beyond the shear critical angle. If acquired with planar transducers instead, such a wide angular coverage would require many measurements.

For the two measurements reported above, the model predictions of the single-CTP model are shown respectively in Fig. 5(c) and (d), whereas the model results according to the multiple-CTP model are shown in Fig. 5(e) and (f), respectively. The single-CTP model results predict well the angular ranges of the experimental results but do not contain the sidelobe effects. The multiple-CTP model results contain interesting

patterns that are likely caused by the sidelobes of both transducers. The experimental results, however, do not show those fine features. The reason needs to be further investigated.

4.2. Reconstruction of the scattering coefficients

As a demonstration of the method, a rapid RC reconstruction is performed on the 1.60-mm-thick aluminum plate using the 2.25 MHz transducers (19.1 mm in diameter and 25.4 mm in focal length). A synthetic-aperture scan is first performed on the aluminum plate sample. The transducer orientation angles are 24°. The x–t domain result is shown in Fig. 6(a). The k–f domain result has been shown in Fig. 5(b) and is repeated in Fig. 6(c) for comparison with later results. To suppress frequency-dependent transducer effects, a second scan is performed on a thick steel block, and this scan is used as a reference for the data. The x–t domain result of the reference scan is shown in Fig. 6(b), and the k–f domain result is shown in Fig. 6(d). The differences between the results of the sample and reference scans are difficult to observe in the x–t domain (shown in Fig. 6(a) and (b)). The differences, however, are very obvious in the k–f domain. The k–f domain result of the sample scan illustrated in Fig. 6(c) shows clearly the plate dispersion spectrum. In the reference scan, because the acoustic impedance of the steel material (used for reference measurement only) is much higher than that of the coupling fluid water, the RC at the water–steel interface is very close to the unity. Therefore, in the k–f domain result of the reference scan in Fig. 6(d) we see mostly the contribution of the transducer beams and the electronic responses rather than the reflection behavior at the water–steel interface. There is, however, the trace of a Rayleigh mode on the surface of the thick steel reference sample in Fig. 6(d), whose effect can be just discerned in the processed data of frame (e). The RC of the immersed plate sample is reconstructed according to

$$R(k,0,f) = \frac{V(k,f)}{V_{\mathrm{ref}}(k,f)} R_{\mathrm{ref}}(k,0,f), \tag{15}$$

where R is the RC of the plate specimen, V and V_{ref} are the k–f domain results of the sample and reference scans, respectively, and R_{ref} is the calculated plane-wave RC based on the known material properties of the steel reference material and the coupling fluid. A Wiener filter (Chen and Sin, 1990) is used when we calculate the RC according to Eq. (15). The result is shown in Fig. 6(e). Here, we see the utility of the reference scan, where the crisscross regions in Fig. 6(c) owing to sidelobe effects at low wave number-frequency are nearly gone. Because our reference sample (thick steel bulk specimen) supports a Rayleigh wave, however, the final result is not perfect. The enhancement from the steel Rayleigh wave can be seen as a bright line following just above the A_0 Lamb mode in Fig. 6(e). For comparison, the calculated plane-wave RC for the aluminum plate immersed in water is shown in Fig. 6(f). It can be seen that within the effective measurement ranges, from 3° to 45° in phase-match angle and from 0.5 MHz to 3.5 MHz in frequency, the theoretical calculation matches the reconstructed RC very well.

The TC of the plate specimen also can be quickly reconstructed in a transmission geometry with focused transducers. An example that demonstrates this variation of our method is given in Fig. 7. The transducers and the plate specimen are the same ones as in the reflection measurement described above. The transducer orientation angles are both 20°, and the measurement scan is first performed on the aluminum plate. A reference scan is then performed under identical experimental conditions, but without the plate sample, assuring that the result contains only the contributions from the transducer frequency response and beam effects.

The x–t domain results from the two scans are shown in Fig. 7(a) and (b), respectively. We see that the data in Fig. 7(a) has more trailing waves than in (b) owing to the presence of the plate. Again, the differences between the two results are shown more clearly in the transformed k–f domain. In the k–f domain result of the sample scan of Fig. 7(c), we see clearly five plate wave modes, A_0, S_0, A_1, S_1, and S_2, whereas in

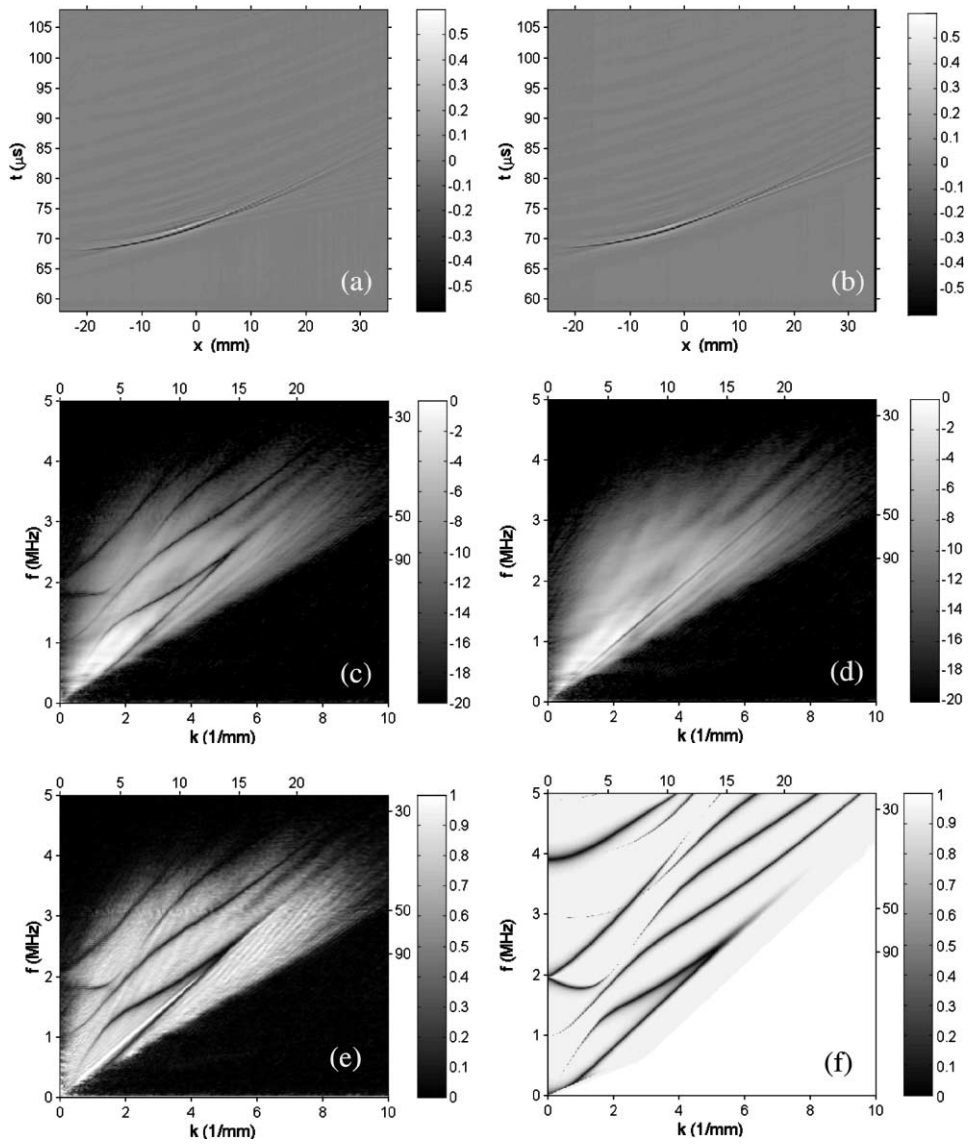

Fig. 6. Rapid reconstruction of the RC on an aluminum plate: (a) x–t domain data in the sample scan, (b) x–t domain data in the reference scan, (c) k–f domain result in the sample scan, (d) k–f domain result in the reference scan, (e) reconstructed RC and (f) calculated plane-wave RC.

the result of the reference scan of Fig. 7(d) this structure is of course absent. In the reflection setup the transducers are prevented by geometry from approaching each other closely at high incident angles. Without this geometric restriction, we are able in transmission to map the dispersion curves for phase-match angles as small as 0°, at the mode cut-offs, and larger than 40°. The reconstructed result is shown in Fig. 7(e), where the grayscale image represents the magnitude of the reconstructed TC on a log scale. The calculated plane-wave TC, based on the elastic property of the sample and coupling fluid, is shown in Fig. 7(f). Again, we see that the experimental and model results are in close agreement.

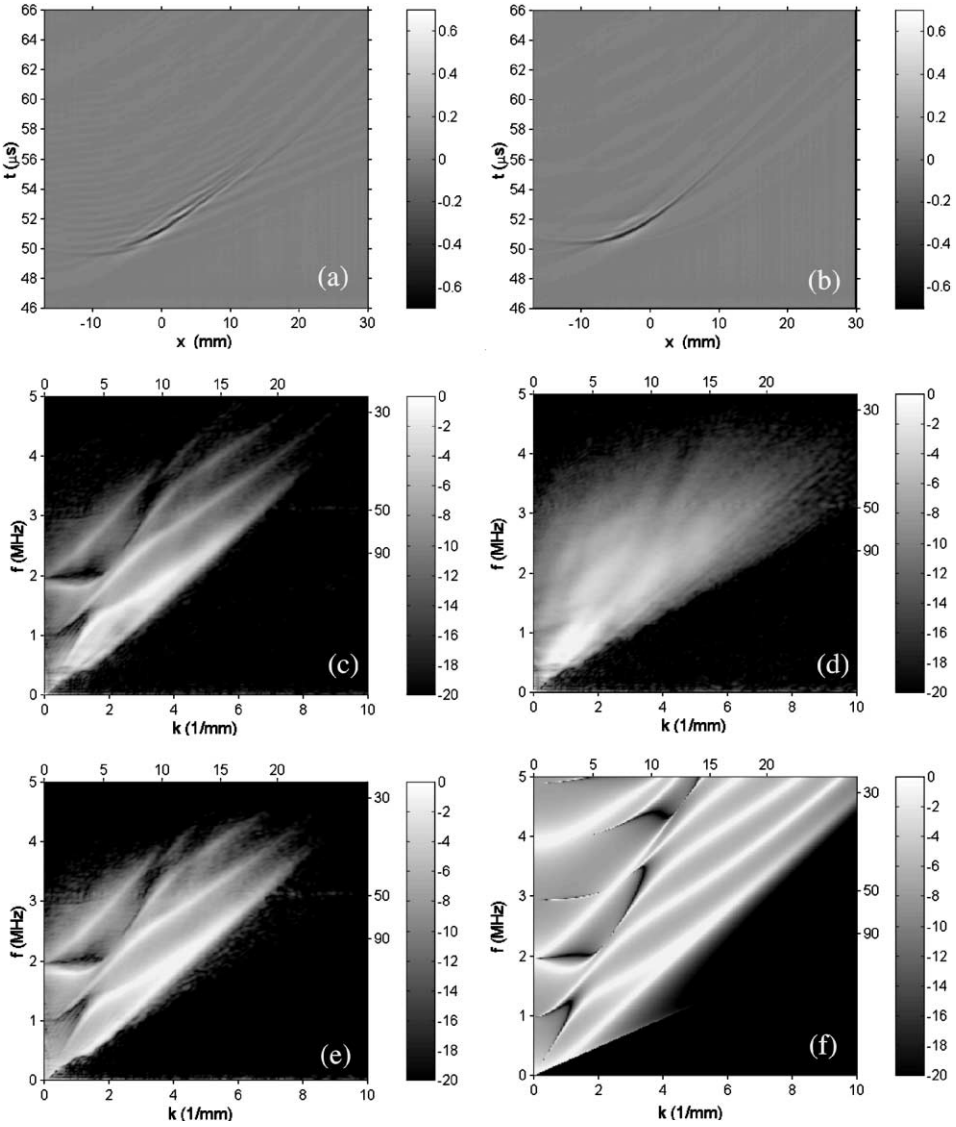

Fig. 7. Rapid reconstruction of the TC on an aluminum plate: (a) sample scan result in the x–t domain; (b) reference scan data in the x–t domain; (c) sample scan result in the k–f domain in dB, (d) reference scan result in the k–f domain in dB, (e) reconstructed TC in dB, and (f) calculated plane-wave TC in dB.

4.3. Elastic property estimation

The SC and its associated dispersion spectrum are the physical quantities that carry the elastic information of the plate material and can therefore be used to reconstruct its elastic properties. We have previously reported a stepwise, targeted procedure (Fei and Chimenti, 2001) to infer elastic stiffnesses from measured dispersion data. In that procedure we concentrate on limited portions of the dispersion spectrum where dependence on elastic properties is limited to one, or only a few, of the full complement of elastic constants. We then proceed to obtain the elastic constants incrementally, beginning with parts of the

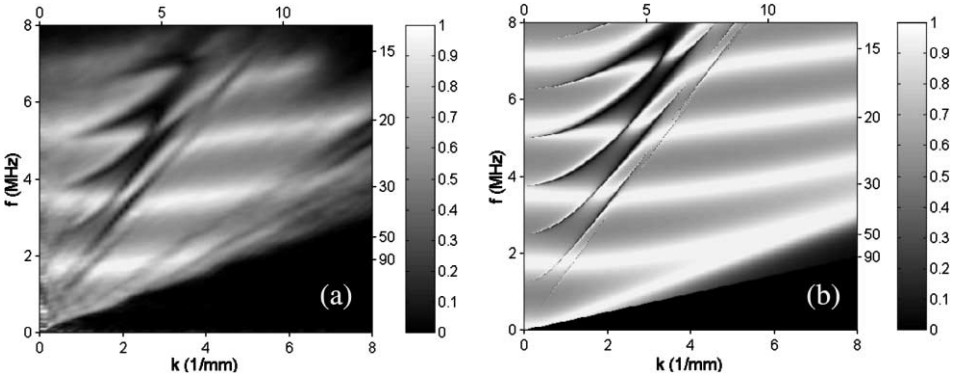

Fig. 8. Elastic property reconstruction along the fiber direction of a uni-axial graphite/epoxy laminate: (a) reconstructed TC in the k–f domain result; (b) calculated TC based on reconstructed elastic constants.

dispersion spectrum where only one, or at most two, stiffnesses affect the plate wave behavior and continue to add data from curves where other constants are active, until all properties have been extracted. We illustrate this method briefly using two simple examples to give an idea of how it functions. A complete exposition of this method and its application will be the subject of a future manuscript.

The first plate specimen is the isotropic aluminum plate that has been used in the above experiments. The reconstructed RC has been shown previously in Fig. 6(e). After running the stepwise dispersion curve based elastic constant reconstruction procedure, we obtain $C_{11} = 54.1$ GPa and $C_{44} = 27.3$ GPa. We have used the two reconstructed elastic constants to calculate the plane-wave RC, which has been shown Fig. 6(f). We see excellent agreement between the measured and calculated results, although we have used only a small, but carefully selected, portion of the RC data to infer the elastic constants of the plate. An independent check using contact probes shows a percentage difference in acoustic velocities of less than 2.0% and 1.0%, respectively, for V_L and V_S. The transmission data given in Fig. 7 can be used just as well to reconstruct the plate's elastic properties.

The second plate sample is a 0.92-mm-thick uniaxial T300/CG-914 $[0]_8$ graphite–epoxy laminate. The material is transversely isotropic with five independent elastic constants, C_{11}, C_{13}, C_{33}, C_{44}, and C_{55}, assuming that the fibers are in the x-direction. Among those elastic constants, C_{11}, C_{13}, C_{33}, and C_{55}, can be determined from a transducer scan in the x-direction, and C_{33} and C_{44} from a scan in the y-direction. The y-direction measurement is in the plane of isotropy and is therefore the same as the isotropic case that has already been discussed. Here, we consider the synthetic aperture scan result in the x-direction only. We have used a pair of 5-MHz cylindrically focused transducers (19.1 mm in diameter and 25.4 mm in focal length) for this specimen, and the measured TC is shown in Fig. 8(a). Using these data and selecting carefully the regions of the dispersion spectrum to employ, we find reconstructed elastic stiffnesses of $C_{11} = 138$ GPa, $C_{13} = 3.3$ GPa, $C_{33} = 15.6$ Gpa, and $C_{44} = 4.3$ GPa. Fig. 8(b) shows the calculated plane-wave TC of the immersed specimen using the above reconstructed elastic parameters. By comparison we see good agreement between the reconstructed and calculated TC. In contact measurements we find estimates that differ from these reconstructed results by less than 3%.

5. Summary and conclusions

By the judicious use of focused probes in a two-transducer reflection or transmission configuration, we have shown that the scattering coefficients can be reconstructed over a wide frequency and wave number

domain from data acquired in a single coordinate scan. To model these results we have employed the complex transducer point approach with multiple sources, leading to an efficient and accurate calculation of the double-transformed data from the experiment. This model has been used to study the k–f domain receiver voltage and to simulate the real transducer effects from all extrinsic experimental parameters including the transducer aperture size, focal length, orientation, and position. Both model and experimental studies have confirmed that the large angular beam spread of the focused transducers can be utilized to obtain a rapid mapping of the plate scattering (reflection or transmission) coefficients and, by extension, their associated dispersion spectra. The measured SC zeroes have been utilized to reconstruct the elastic properties of the plate material through a targeted procedure that eliminates from consideration most of the highly redundant dispersion data. Experiments have been performed on both isotropic and anisotropic plates, and the results show a deviation of less than 3% from contact acoustic estimates. This method provides a rapid, accurate, and simple alternative to the use of electronically steered arrays or to mechanical steering of planar transducer beams for material property estimation in thin plates. Although all the model and experimental study in this work has been limited to the water-coupled reflection or transmission measurements, the same principles are completely applicable to similar measurements with any coupling medium, such as air, for material property estimation in plates.

Acknowledgements

This work has been supported in part by the Institute for Physical Research and Technology at Iowa State University and in part by the US Navy under contract N00167-00-M-0694. The authors gratefully acknowledge Drs. R.B. Thompson, H. Zhang, and O.I. Lobkis for helpful discussions on modeling and S.V. Teles for assistance with some of the experiments. The authors also thank Dr. D.K. Hsu for the loan of some of the transducers for this work.

References

Alleyne, D., Cawley, P., 1991. A two-dimensional Fourier transform method for the measurement of propagating multimode signals. J. Acoust. Soc. Am. 89, 1159–1168.

Auld, B.A., 1979. General electro-mechanical reciprocity relations applied to the calculation of elastic wave scattering coefficients. Wave Motion 1, 3–10.

Chen, C.H., Sin, S.K., 1990. On effective spectrum-based ultrasonic deconvolution techniques for hidden flaw characterization. J. Acoust. Soc. Am. 87 (3), 976–987.

Chimenti, D.E., 1997. Guided waves in plates and their use in materials characterization. Appl. Mech. Rev. 50, 247–284.

Chimenti, D.E., Zhang, J., Zeroug, S., Felsen, L.B., 1994. Interaction of acoustic beams with fluid-loaded elastic structures. J. Acoust. Soc. Am. 95, 45–59.

Deschamps, G.A., 1971. Gaussian beam as a bundle of complex rays. Electron. Lett. 7, 684–685.

Deschamps, M., Hosten, B., 1992. The effects of viscoelasticity on the reflection and transmission of ultrasonic waves by an orthotropic plate. J. Acoust. Soc. Am. 91, 2007–2015.

Fei, D., 2001. Lay-up characterization and elastic property determination in composite laminates. Ph.D. dissertation, Iowa State University, USA.

Fei, D., Chimenti, D.E., 2001. Single-scan elastic property estimation in plates. Acoust. Res. Lett. Online 2 (1), 49–54.

Gavrilov, L.R., Dmitriev, V.N., Solontsova, L.V., 1988. Use of focused ultrasonic receivers for remote measurements in biological issues. J. Acoust. Soc. Am. 83 (3), 1167–1179.

Hosten, B., Deschamps, M., Tittmann, B.R., 1987. Inhomogeneous wave generation and propagation in lossy anisotropic solids: application to the characterization of viscoelastic composite materials. J. Acoust. Soc. Am. 82, 1763–1770.

Hosten, B., Hutchins, D.A., Schindel, D.W., 1996. Measurement of elastic constants in composite materials using air-coupled ultrasonic bulk waves. J. Acoust. Soc. Am. 99, 2116–2123.

Hsu, D.K., Margetan, F.J., 1992. Analysis of acousto-ultrasonic signals in unidirectional thick composites using the slowness surfaces. J. Comp. Mat. 26, 1050–1061.

Karim, M.R., Mal, A.K., BarCohen, Y., 1990. Inversion of leaky Lamb wave by simplex algorithm. J. Acoust. Soc. Am. 88, 482–491.

Karunasena, W., Bratton, R.L., Datta, S.K., Shah, A.H., 1991. Elastic wave propagation in laminated composite plates. J. Eng. Mat. Tech. 113, 411–418.

Kino, G.S., 1978. The application of reciprocal theory to scattering of acoustic waves by flaws. J. Appl. Phys. 49, 3190–3199.

Kolosov, O.V., Yamanaka, K., Lobkis, O.I., Zinin, P.V., 1993. Evaluation of a point-spread function of focussing systems using a spherical reflector. In: Ultrasonics International-93. Butterworth-Heinemann, Oxford, pp. 547–550.

Levin, V.M., Lobkis, O.I., Maev, R.G., 1990. Investigation of the spatial structure of acoustic fields by a spherical focusing transducer. Sov. Phys. Acoust. 36 (4), 391–395.

Lobkis, O.I., Safaeinili, A., Chimenti, D.E., 1996. Precision ultrasonic reflection studies in fluid-coupled plates. J. Acoust. Soc. Am. 99, 2727–2736.

Lobkis, O.I., Chimenti, D.E., 1999. Three-dimensional transducer voltage in anisotropic materials characterization. J. Acoust. Soc. Am. 106, 36–45.

Lobkis, O.I., Chimenti, D.E., Zhang, H., 2000. In-plane elastic property characterization in composite plates. J. Acoust. Soc. Am. 107, 1852–1857.

Minachi, A., Hsu, D.K., Thompson, R.B., 1994. Single-sided determination of elastic constants of thick composites using acousto-ultrasonic technique. J. Acoust. Soc. Am. 96, 353–362.

Rogers, W.P., 1995. Elastic property measurement using Rayleigh–Lamb waves. Res. Nondestruct. Eval. 6, 185–192.

Rohklin S.I, Chimenti, D.E., 1990. Reconstruction of elastic constants from ultrasonic reflectivity data in a fluid-coupled composite plate. In: Thompson, D.O., Chimenti, D.E. (Eds.), Review of Progress in Quantitative Nondestructive Evaluation, vol. 9. Plenum, New York, pp. 1411–1418.

Rokhlin, S.I., Wang, W., 1992. Double through-transmission bulk wave method for ultrasonic phase velocity measurement and determination of elastic constants of composite materials. J. Acoust. Soc. Am. 91, 3303–3312.

Sachse, W., Pao, Y.H., 1978. On the determination of phase and group velocities of dispersive waves in solids. J. Appl. Phys. 49, 4320–4327.

Safaeinili, A., Lobkis, O.I., Chimenti, D.E., 1996. Air-coupled ultrasonic estimation of viscoelastic stiffness in plates. IEEE Trans. Ultrason. Ferroelectr. Freq. Control 43, 1171–1180.

Schmerr Jr., L.W., 1998. Fundamentals of ultrasonic nondestructive evaluation: a modeling approach. Plenum Press, New York.

Thompson, R.B., Lopes, E.F., 1984. The effects of focussing and refraction on Gaussian ultrasonic beams. J. NDE 4 (2), 107–123.

Veidt, M., Sachse, W., 1994. Ultrasonic evaluation of thin, fiber-reinforced laminates. J. Compos. Mater. 28, 329–342.

Weaver, R.L., Sachse, W., Niu, L., 1989. Transient ultrasonic waves in a viscoelastic plate: applications to materials characterization. J. Acoust. Soc. Am. 85, 2262–2267.

Wen, J.J., Breazeale, M.A., 1988. A diffraction beam field expressed as the superposition of Gaussian beams. J. Acoust. Soc. Am. 83, 1752–1756.

Yang, C.H., Chimenti, D.E., 1995. Guided plate waves in piezoelectric immersed in a dielectric fluid I. Analysis. J. Acoust. Soc. Am. 97, 2103–2109.

Zeroug, S., Felsen, L.B., 1994. Nonspecular reflection of two-and three-dimensional acoustic beams from fluid-immersed plane-layered elastic structures. J. Acoust. Soc. Am. 95, 3075–3098.

Zeroug, S., Felsen, L.B., 1995. Nonspecular reflection of two-and three-dimensional acoustic beams from fluid-immersed cylindrically layered elastic structures. J. Acoust. Soc. Am. 98, 584–598.

Zeroug, S., Stanke, F.E., Burridge, R., 1996. A complex-transducer-point model for emitting and receiving ultrasonic transducers. Wave Motion 24, 21–40.

Zhang, H., Chimenti, D.E., Zeroug, S., 1998. Transducer misalignment effects in beam reflection from elastic structures. J. Acoust. Soc. Am. 104, 1982–1991.

Zhang, H., Chimenti, D.E., 2000. Two- and three-dimensional complex-transducer-point analysis of beam reflection from anisotropic plates. J. Acoust. Soc. Am. 108, 1–9.